Microchimica Acta (2021) 188: 237
https://doi.org/10.1007/s00604-021-04895-x

ORIGINAL PAPER

An "off-on" electrochemiluminescence biosensor coupled with strand displacement-powered 3D micromolecule walking nanomachine for ultrasensitive detection of adenosine triphosphate

Li Li[1] · Zheng Zhou[2] · Xinmin Li[3,4] · Dandan Li[3] · Min Zhao[3] · Changjin Liu[3] · Haiping Wu[3] · Wei Yang[3] · Shijia Ding[3] · Bo Shen[3,4]

Received: 25 March 2021 / Accepted: 12 June 2021 / Published online: 28 June 2021

Abstract

A three-dimensional (3D) micromolecule walking nanomachine propelled by strand displacement was developed to establish a novel switching electrochemiluminescence (ECL) biosensor for ultrasensitive detection of adenosine triphosphate (ATP). Generally, walking nanomachines reported previously were limited to DNA walkers, while the proposed 3D walking nanomachine focused on the micromolecule walker. Firstly, TiO_2 and silver nanoparticles (Ag NPs) functionalized N-(4-aminobutyl)-N-(ethylisoluminol) (Ag-ABEI) were deposited onto the electrode surface to offer an enhanced ECL signal, resulting from the double catalytic effect of TiO_2 and Ag NPs for H_2O_2. Following, dopamine (DA)-labeled DNA duplex probes (S1/S2-DA) immobilized onto the modified electrode cut down the original ECL signal due to the quenching of DA toward ABEI (signal-off). Target ATP walker moved along the 3D DNA track, simultaneously releasing numerous DNA3, which was applied to displace S2-DA, resulting in the quenched ECL intensity recovery (signal-on). As a result, the biosensor showed a low limit of detection down to 0.5 nM (S/N = 3) and was successfully employed to determine ATP in human serum samples. Thus, the established biosensing strategy holds great potential for biochemical studies and clinical diagnosis.

Keywords Electrochemiluminescence; Biosensor · Nanomachine · Strand displacement · Switching signal · Adenosine triphosphate determination

Introduction

Adenosine triphosphate (ATP), the direct energy currency in living species, plays crucial roles in cellular metabolic processes and various biochemical reactions, including DNA/RNA biosynthesis, neurotransmission, and muscle contraction [1–3]. ATP concentration in normal human serum is very low (below 28 nM) [4]. Increasing pieces of evidence have shown that ATP can be a marker of cell injury and viability, and abnormal concentration is closely related to parkinsonism, alzheimer's, and cardiovascular diseases [5, 6]. Considering its unique functions, accurate recognition and detection of ATP are of indispensable significance for biochemical studies and diagnosis of disease. Until now, many analytical strategies for ATP detection, including mass spectrometry [7], high-performance liquid chromatography [8], fluorescence [9], and electrochemistry [10], have been developed. Though having achieved sensitive detection of ATP assay, these methods suffered from at least one disadvantage of tedious sample preparation, expensive instruments, and high cost, which limited their wide applications [11, 12]. Thus, it is a great demand to construct rapid, cost-effective, and ultrasensitive strategies to detect ATP in clinical samples.

Electrochemiluminescence (ECL) strategies have been extensively constructed and applied in trace analysis, given the

Li Li and Zheng Zhou contributed equally to this work.

✉ Bo Shen
shenboszy228@163.com

[1] Department of Laboratory Medicine, Chongqing General Hospital, University of Chinese Academy of Sciences, Chongqing 400014, China

[2] Department of Laboratory Medicine, Chongqing University Three Gorges Hospital, Chongqing 404000, China

[3] Key Laboratory of Clinical Laboratory Diagnostics (Ministry of Education), College of Laboratory Medicine, Chongqing Medical University, Chongqing 400016, China

[4] Department of Laboratory Medicine, Chongqing Hospital of Traditional Chinese Medicine, Chongqing 400021, China

merits of high sensitivity and specificity, simplified operation, and low cost [13–15]. As the derivative of luminol, the ABEI/hydrogen peroxide (H_2O_2) system has been widely used as an ECL reaction system owing to the nontoxicity, low oxidation, and high luminous efficacy [16, 17]. Moreover, the ABEI is tagged easily with another reagent for constructing an enhanced luminophore. For example, MoS_2 nanoflowers [18], TiO_2 nanoflowers [19], and Ag nanoparticles (Ag NPs) [20] could serve as effective co-reaction accelerators of ABEI/H_2O_2 for the decomposition of H_2O_2 to produce amounts of superoxide radical ($O_2^{\bullet-}$) and hydroxyl radical ($OH^{\bullet}$), which could oxidize ABEI to obtain an amplified ECL intensity. However, in most reported ECL biosensors, the common methods to detect targets only depend on the "signal-on" or "signal-off" of the ABEI, which leads to false-positive response resulting from interfering substance in biological fluid [21]. Recently, the "off-on" mode ensures ECL biosensors with superior abilities of higher signal-to-noise ratio, which offers a robust approach for ATP detection in ABEI/H_2O_2 system [22, 23].

Molecular machines, widespread existing in living organisms, can perform various physiological functions in response to surrounding change stimulus [24, 25]. Such natural phenomenon has inspired enormous interests in constructing advanced nanomachines for biosensing, such as walking nanomachines, tweezers, and molecular gears [26–28]. Particularly, walking nanomachines in which walkers move autonomously and sequentially along the preset three-dimensional (3D) DNA tracks impelled by DNAzyme, protease, and strand displacement have been widely used to biomarker analysis [29–32]. Generally, strand displacement is considered as a promising driver that drive walkers' motion without being tampered with by environmental factors [33]. Moreover, the reports about molecular nanomachines in recent years are limited to one dimensional (1D) or two dimensional (2D) nanostructure, and the effects of cargoes transit are unsatisfactory due to the inadequate ability of 1D or 2D walking space and low fluxes of the substrate [34]. Nowadays, these 3D nanomachines enable the rapid transduction of trace target information into a great quantity of detectable signals owing to their extraordinary motion efficiency, highly local concentration of DNA track, and unique programmability [35, 36]. Nevertheless, nearly all researched walking nanomachines are restricted to DNA walkers [37]. Small molecules or proteins walkers have been barely reported due to the great challenge of how to effectively push their movement from one to another adjacent DNA track.

Inspired by the concepts above, toehold strand displacement-powered 3D micromolecule walking nanomachine was established for the first time, which further integrated with Ag NP-functionalized ABEI (Ag-ABEI) and TiO_2-modified

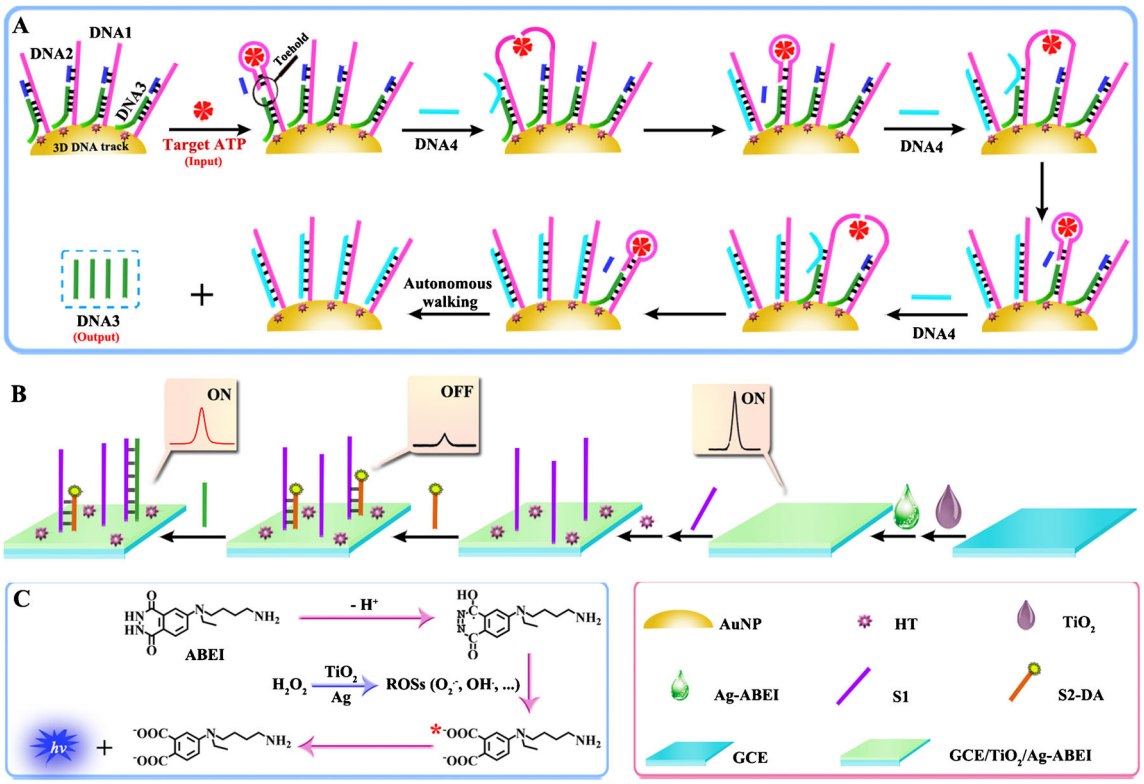

Scheme 1 Principle of the ECL biosensor coupled with toehold strand displacement-powered 3D micromolecule walking nanomachine for the detection of ATP. **A** Schematics for 3D micromolecule walking nanomachine. **B** The fabrication process of the developed ECL biosensor. **C** The probable mechanism of the established biosensor

electrode matrix to establish switching ECL biosensor for sensitive detection of ATP assay (Scheme 1). For process A, ATP captured by aptamer moved autonomously along the 3D DNA track powered by strand displacement, leading to the output of the numerous DNA3. For process B, the TiO_2/Ag-ABEI was first immobilized onto the electrode surface to produce an enhanced ECL intensity, because of the dual decomposition of TiO_2/Ag NPs toward H_2O_2. Next, DNA duplex probes tagged with dopamine (DA) (S1/S2-DA) were assembled on the modified electrode, leading to the prominent reduction of the initial ECL response due to the quenching effect of DA for ABEI (signal-off). Then, S2-DA was displaced by the released DNA3, resulting in the recovery of the ECL signal (signal-on). Therefore, the established "off-on" ECL biosensor offered a simple strategy for ultrasensitive ATP analysis, contributing to biochemical studies and clinical diagnosis of diseases.

Experimental

Materials and reagents

All DNA sequences (Table S1) were synthesized and purified by Sangon Biotechnology Co., Ltd. (Shanghai, China, http://www.sangon.com/). The oligonucleotides were dissolved in TE buffer (10 mM Tris-HCl, 1 mM ethylenediaminetetraacetic acid (EDTA), pH 8.0). ATP, cytidine triphosphate (CTP), thymine triphosphate (TTP), and guanosine triphosphate (GTP) were purchased from Worthington Biochemicals Co., Ltd. (Lakewood, NJ, USA, https://worthington.guidechem.com/). Hexanethiol (HT), gold chloride tetrahydrate ($HAuCl_4 \cdot 4H_2O$), and ABEI were obtained from Sigma-Aldrich Co., Ltd. (St. Louis, MO, USA, http://www.sigmaaldrich.com/). N-Hydroxysuccinimide (NHS) and 1-(3-dimethylaminopropyl)-3-ethylcarbodiimide hydrochloride (EDC) were obtained from Shanghai Medpep Co., Ltd. (Shanghai, China, http://www.medpep.com/). Tetrabutyl titanate ($Ti(OC_4H_9)_4$) was purchased from Sinopharm Chemical Reagent Co., Ltd. (Shanghai, China, http://en.reagent.com.cn/). H_2O_2 (30%), ethanol, $AgNO_3$, and other reagents were purchased from Chemical Reagent Co., Ltd. (Chongqing, China, https://chuandong.lookchem.com/). All chemicals were of analytical grade, and all experiments were prepared using ultrapure water obtained from a Millipore water purification system (≥ 18.2 MΩ/cm, MA, USA, http://www.mollipore.com/). Phosphate buffer solution (PBS, 0.1 M, containing 2 mM $MgCl_2$ and 10 mM KCl, pH 8.0) was used as the working buffer. Twenty millimolar mM Tris-HCl buffer (pH 7.4) containing 1 mM $MgCl_2$, 1 mM $CaCl_2$, 5 mM KCl, and 140 mM NaCl was used as the binding buffer solution.

Apparatus

Electrochemical measurement was monitored by a CHI 660E electrochemistry workstation (Shanghai Chenhua Instruments Co., Ltd, Shanghai, China, http://www.chinstruments.com/). The ECL emissions were monitored with a MPI-A ECL analyzer (Xi'an Remax Electronic Science & Technology Co., Ltd, Xi'an, China, http://www.chinaremex.com/). The ultraviolet-visible (UV-vis) spectrophotometer (Shimadzu, Kyoto, Japan, http://www.shimadzu.com/), scanning electron microscope (SEM), transmission electron microscopy (TEM) (Hitachi, Tokyo, Japan, https://www.hitachi.com/), and X-ray photoelectron spectroscopy (XPS) (Thermo, Waltham, MA, USA, https://www.thermofisher.cn/) were applied to characterize the features and morphologies of nanomaterials.

Fabrication of 3D micromolecule walking nanomachine

First, the Au NPs were obtained based on the previous method with some modifications (see the Electronic Supporting Material for details). Second, the aptamer strand (DNA1, 500 nM) and Au NPs (1% w/w) were bonded in 100 μL of Tris-HCl buffer overnight at room temperature (RT) via an Au-N bond to form DNA1-Au, and the mixture was "aged" in 1 M NaCl for another 12 h. Subsequently, the solution was centrifuged at 12,000 rpm for 10 min to remove the excess reagents. Third, the centrifugal product was resuspended in 100 μL of Tris-HCl buffer; HT (1 mM) was used to block the redundant binding sites. Then, a helper strand (DNA2, 500 nM) and output strand (DNA3, 500 nM) were added and heated to 90 °C for 5 min, followed by slowly cooling down to RT. Thus, the DNA1/DNA2/DNA3 three-strand could be tethered to the surface of Au NPs, forming a 3D DNA track. The unreacted DNA1, DNA2, and DNA3 were removed by centrifugation. Finally, different concentrations of ATP and the fuel probes (DNA4, 500 nM) were introduced to the 3D DNA track with a reaction volume of 50 μL and incubated for 80 min at RT to perform the motion of ATP walker and achieve the output of DNA3.

Construction of the switchable "off-on" ECL biosensor

The synthetic of TiO_2 and Ag-ABEI nanoparticles was depicted in the Electronic Supporting Material (ESM). The S2-DA composite was firstly obtained as follows: First, 25 μL of S2 (100 μM) was added into 1 mL of PBS (0.1 M, pH 7.4), then adding EDC (20 mM) and NHS (5 mM), stirring for 1 h at RT to activate the carboxyl of S2. Subsequently, 200 μL of DA solution (100 μM) was added into the planned S2 mixture with stirring overnight at 4 °C to obtain the S2-DA products. Before modification, the bare GCE was polished

with 0.3 and 0.05 μm alumina slurry, followed by sonication with ultrapure water. Then, 10 μL of TiO_2 and Ag-ABEI nanoparticles were successively spread on the cleaned GCE surface to form a well-dispersed nanofilm. In this case, the TiO_2/Ag-ABEI nanoparticles could doubly catalyze H_2O_2 by generating a lot of free radicals, which could further oxidize ABEI for the enhanced ECL emission. Ten microliters of 2.5 μM S1 was immobilized onto the TiO_2/Ag-ABEI nanofilm overnight via an Ag-N bond, and the modified electrode was blocked with 1.0 mM HT for 40 min. Subsequently, 10 μL of S2-DA was dropped on the electrode surface and reacted for 2 h at RT to hybridize with S1. The unbound S2-DA was eliminated by washing three times with ultrapure water. Then, 10 μL of the output DNA3 released by the 3D micromolecule walking nanomachine was incubated with the resulting electrode for 2 h. After that, the electrode was tested by an ECL analyzer. Ultrapure water was utilized to wash the modified electrode after each fabrication step, and the obtained electrode was kept at 4 °C for further use. Finally, the obtained biosensor was detected in the buffer of 2 mL PBS (0.1 M, pH 8.0) containing H_2O_2 (3 mM) at room temperature to investigate the ECL response. The ECL intensity was gained by a MPI-A ECL analyzer with working potential from 0 V to 0.6 V (vs. Ag/AgCl) at a scan rate of 0.1 V/s and the voltage of the photomultiplier tube (PMT) at 800 V.

Result and discussion

Principle of the biosensor

The detection principle of the biosensor based on toehold strand displacement-powered 3D walking nanomachine for detection of ATP in an "off-on" manner is illustrated in Scheme 1. As illustrated in Scheme 1A, the designed 3D micromolecule walking nanomachine consisted of three aspects: target ATP as a walker, three-strand DNA complex (DNA1/DNA2/DNA3) immobilized on the same Au NPs as walking 3D DNA track, and DNA4 as drive chain. DNA1 (pink color) contained an aptamer sequence that was used to capture the target ATP. DNA2 (blue color) and DNA3 (green color) were initially hybridized with DNA1 to block the toehold region, and DNA3 acted as the output strand. In the presence of the target ATP, which bound to the DNA1 and changed its conformation, triggering the release of DNA2 and the exposure of a 4 nt toehold domain (Fig. S1). Then, DNA4 hybridized with DNA1 beginning from the exposed toehold domain and simultaneously displaced ATP and DNA3, and the freed ATP again bound to the next adjacent track. In a manner, the ATP walker moved autonomously along the engineered 3D track, leading to the release of many DNA3. As showed in Scheme 1B, the treated GCE was deposited with TiO_2/Ag-ABEI nanoparticles, followed by the assembly of a DNA sequence (S1). Next, HT is used to block the nonspecific binding sites, followed by the hybridization of S2-DA and S1. Therefore, the ECL intensity was decreased because of the quenching effect of DA toward ABEI (signal-off). Furthermore, the released DNA3 was immersed onto the pretreated electrode to displace S2-DA (signal-on). The ECL mechanism was depicted in Scheme 1C; TiO_2/Ag NPs could exhibit the double catalytic effect toward H_2O_2 to generate a good deal of ROSs ($O_2^{\bullet-}$ and $OH^{\bullet}$), which improved the ECL reaction rate of ABEI with high intensity. In general, combining the 3D micromolecule walking nanomachine with TiO_2/Ag-ABEI-coated electrode, an "off-on" ECL biosensor has been successfully developed, which offers a novel and effective tool for ultrasensitive detection of ATP.

Characterization of the Au NPs and TiO_2 nanoflowers

To confirm the homogeneous and spherical structure of the synthesized Au NPs with an average size of 13 ± 2 nm, the TEM image of the Au NPs was displayed in Fig. 1A. Subsequently, XPS characterization was performed to verify the integrated preparation of DNA1-Au NP composites via elemental analysis. As shown in Fig. 1B, the peaks at 532, 399, and 285 eV belonged to O1s, N1s, and C1s, respectively. Additionally, the doublets at 88 and 84 eV were assigned to Au 4f. In Fig. 1C, the binding energies for Au $4f_{7/2}$ and Au $4f_{5/2}$ located at 83.7 and 87.4 eV, respectively, which proved the presence of an Au-N bond. Moreover, the UV-vis absorption spectra of the Au NPs-DNA1 conjugates were shown in Fig.1D. AuNPs exhibited an absorption peak at 520 nm (curve a), while the UV-vis absorption spectra of AuNPs-DNA1 were redshifted to 525 nm (curve b). The insets of Fig. 1D showed the corresponding photographs, which were in accordance with results obtained by UV-vis absorption spectra. These results demonstrated that the loading of DNA1 on AuNPs was successfully achieved.

Furthermore, the SEM image of the synthesized TiO_2 nanoflowers was shown in Fig. 1E. It demonstrated that the TiO_2 nanoflowers had a flower-like structure with an average diameter of 2.0 ± 0.5 μm. In Fig. 1F, the UV-vis absorption spectra were performed to confirm the synthesis of Ag-ABEI nanoparticles. ABEI had a characteristic absorption peak at 292 nm; the Ag-ABEI nanoparticles showed a new absorption band around 442 nm when associated with the Ag NPs (393 nM). These results indicated that TiO_2 nanoflowers and Ag-ABEI nanoparticles were successfully synthesized.

ECL characterization of the biosensor

To demonstrate the process of electrode modification, ECL signals were monitored. As shown in Fig. 2A, the bare GCE and the TiO_2 nanoflower-modified electrode obtained an ignorable ECL signal corresponding to curve a and b,

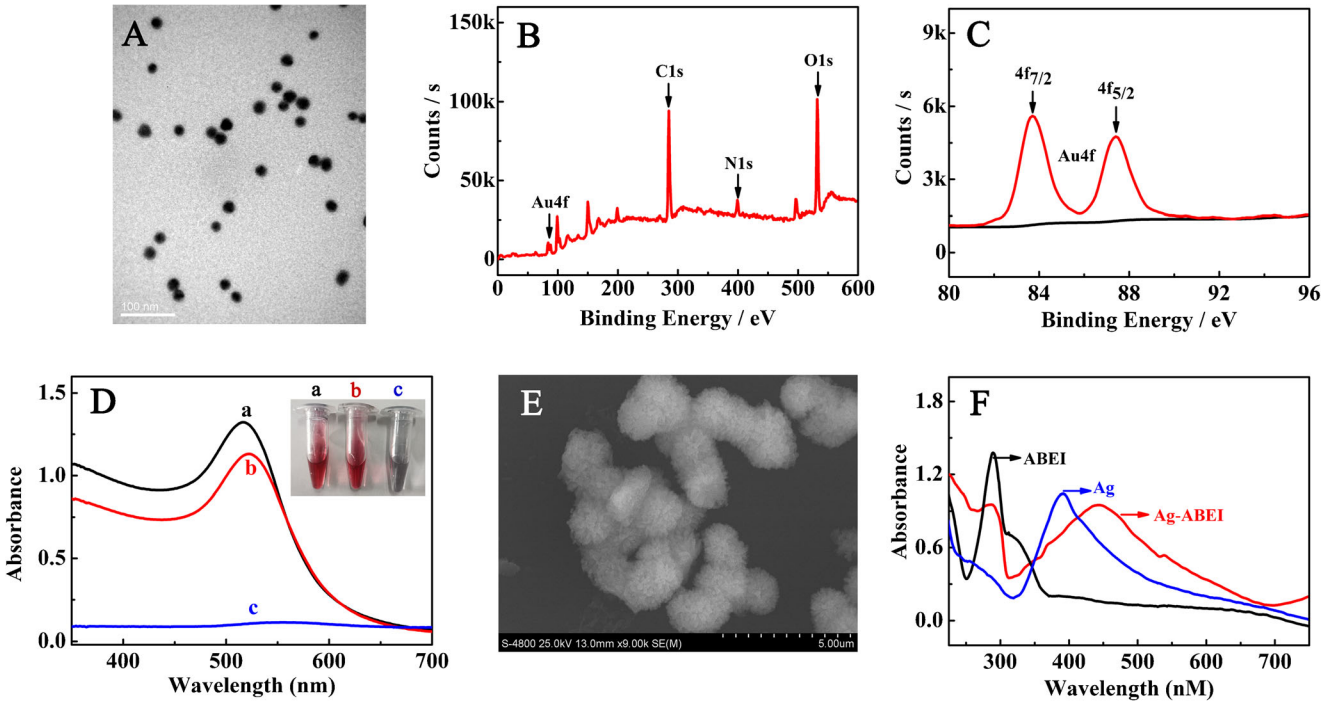

Fig. 1 **A** TEM image of Au NPs. Scale bar, 100 nm. **B** XPS analysis for the full region of XPS for NH_2-DNA1 functionalized Au NPs. **C** XPS spectra of Au 4f region. **D** UV-vis absorption spectra of (a) bare Au NPs, (b) NH_2-DNA1 functionalized Au NPs after addition of 1 M NaCl, (c) bare Au NPs after addition of 1 M NaCl (insets: the corresponding photographs). **E** SEM image of TiO_2 nanoflowers. Scale bar, 5.0 μm. **F** UV-vis absorption spectra of ABEI, Ag NPs, and Ag-ABEI

respectively. Furthermore, when the Ag-ABEI nanoparticles were deposited onto the surface of the electrode, a strong ECL signal was obtained (curve c), while the ECL response reduced continually upon the binding of the S1 probe (curve d) and HT (curve e) to the electrode. Subsequently, the introduction of S2-DA led to extremely weak ECL emission owing to the quenching of DA toward the ECL signal of ABEI (curve f). However, the ECL signal obviously improved after DNA3 displaced S2-DA (curve g). These results demonstrated that the switching biosensor was feasible.

In addition, the dual-catalytic effect of TiO_2 and Ag NPs toward H_2O_2 was evaluated. As shown in Fig. 2B, the ECL responses produced by different metal nanostructures followed the order of TiO_2/Ag-ABEI > TiO_2-ABEI > Ag-ABEI > ABEI. Specifically, the ABEI-deposited GCE produced about 2255 a.u. (curve a), the Ag-ABEI-coated GCE generated about 4708 a.u. (curve b), and the TiO_2-ABEI-coated GCE obtained about 7821 a.u. (curve c), but the TiO_2/Ag-ABEI-assembled GCE showed a tremendous increase of ECL intensity about 12563 a.u. (curve d). The results indicated that TiO_2/Ag NPs could exhibit the double catalytic effect toward H_2O_2 to generate a good deal of ROSs ($O_2^{\bullet-}$ and $OH^{\bullet}$), which improved the ECL reaction rate of ABEI with high intensity.

Cyclic voltammetric (CV) and electrochemical impedance spectroscopy (EIS) were used to characterize the stepwise modification process of the electrode; the results indicated that the biosensor was successfully constructed (Fig. S2 in the ESM).

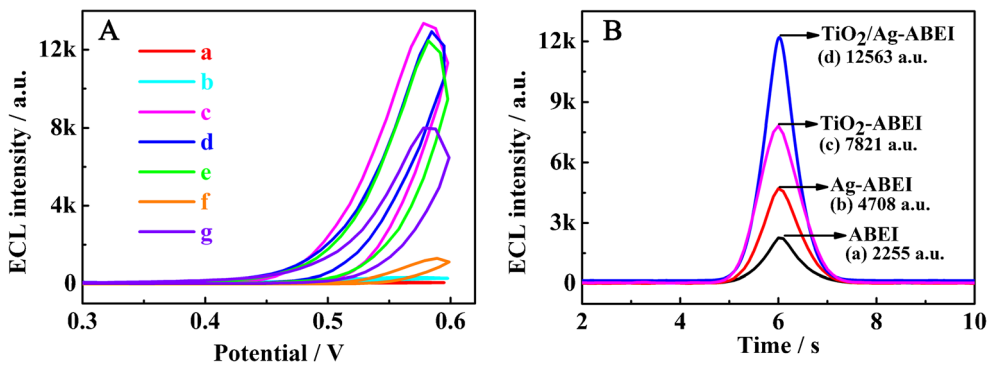

Fig. 2 **A** ECL intensity for each modified step: (a) bare GCE, (b) GCE/TiO_2, (c) GCE/TiO_2/Ag-ABEI, (d) S1 immobilized on GCE/TiO_2/Ag-ABEI, (e) HT blocking, (f) incubated with S2-DA, (g) DNA3 replacing S2-DA. **B** ECL signal responding to (a) ABEI, (b) Ag-ABEI, (c) TiO_2-ABEI, (d) TiO_2/Ag-ABEI. The tests were performed in 2 mL PBS (pH 8.0) containing 3 mM H_2O_2

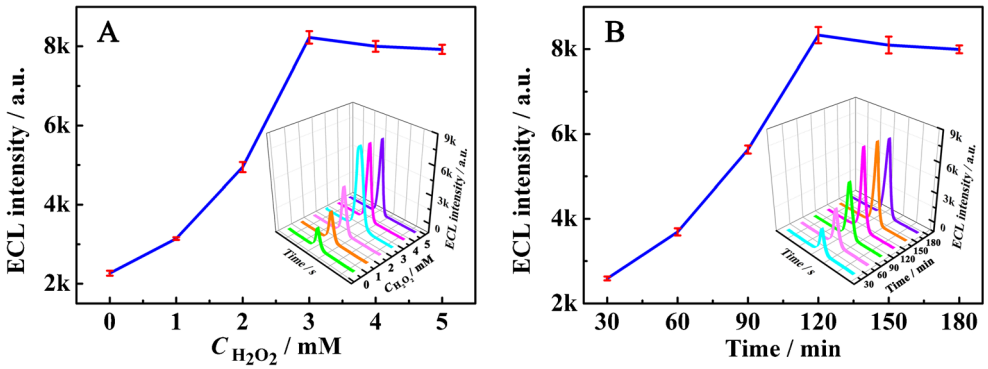

Fig. 3 **A** The effect of the concentration of H_2O_2 on the biosensor. **B** Influence of the incubation time of DNA3 and S1/S2-DA

Optimization of conditions

To gain a high-performance biosensor, experimental conditions including the concentration of H_2O_2 and the incubation time of output DNA3 and S1/S2-DA were investigated. Owing to the great influence of H_2O_2 as a co-reactant of ABEI on the ECL efficiency, the optimal concentration of H_2O_2 was first investigated. As shown in Fig. 3A, the ECL signal consecutively increased with the increase of H_2O_2 concentration and reached a peak value at 3 mM. Therefore, the concentration of H_2O_2 was fixed at 3 mM. Then, the incubation time of output DNA3 and S1/S2-DA was optimized to evaluate effective assay time. As shown in Fig. 3B, ECL intensity experienced an upward trend with the increase of the incubation time from 30 to 120 min. However, the ECL signal increased slowly when the reaction time exceeded 120 min, suggesting the hybridization reaction had saturated. Therefore, 120 min was chosen as the optimum hybridization time.

Analytical performance

To evaluate the sensitivity of the biosensor, different concentrations of ATP were tested under the optimal reaction conditions. Figure 4A depicted the good linear relationship between the ECL signal and ATP concentrations in the range of 1.0 nM to 78.1 μM. As shown in Fig. 4B, a regression equation between the ECL intensity and the logarithm (lg) of the ATP concentration was expressed as I = 1374.0 lgc + 1766.4 (R = 0.9988), in which *I* stands for ECL intensity, *c* represents ATP concentration. The limit of detection (LOD) was estimated to be 0.5 nM at a signal-to-noise of 3. Compared with the previously reported methods for ATP (Table S2), the biosensor showed a lower LOD, which was attributed to superior "off-on" reaction mode, effective micromolecule walking nanomachine, and excellent TiO_2/Ag-ABEI luminophore. Meanwhile, these results demonstrated that the "off-on" system possessed the merits of obvious signal-to-noise ratio, high sensitivity, and wide range of detection. Therefore, the biosensor was a potential tool for highly sensitive ATP analysis.

Reproducibility, stability, and selectivity of the biosensor

First, the reproducibility of the biosensor was evaluated using the relative standard deviations (RSD) of the ECL signal for three concentrations (15 nM, 125 nM, and 1 μM) of ATP in various batches. The RSD were successively calculated to be 0.55%, 1.38%, and 3.27% (n = 3). Therefore, the developed biosensor had the desired reproducibility. Second, the stability of the biosensor was studied at different concentrations of ATP. As depicted in Fig. 5A, the ECL curves retained

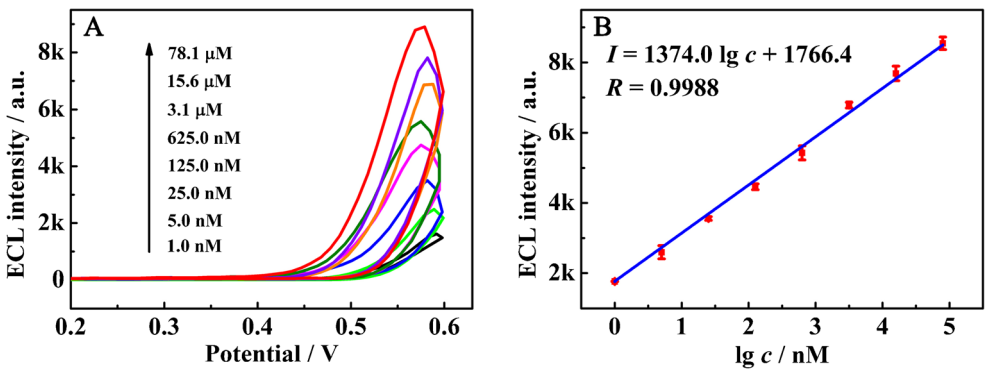

Fig. 4 Evaluation of the analytic property of the proposed ECL biosensor. **A** ECL intensity responding to different concentrations of ATP. **B** The calibration plots for ATP detection. The error bars were the standard deviation of three repetitive experiments. All the ECL tests were performed in 2 mL of PBS (pH 8.0) containing 3 mM H_2O_2

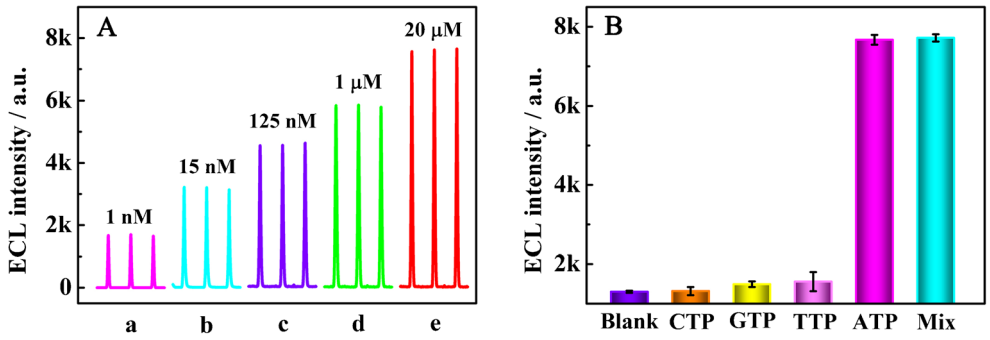

Fig. 5 **A** Evaluation of the stability of the ECL biosensor: ECL intensity responding to various concentrations of ATP. **B** Evaluation of the specificity of the ECL biosensor: Blank, CTP (100 μM), GTP (100 μM), TTP (100 μM), ATP (20 μM), and a mixture (Mix)

relatively stable at each concentration of ATP. This indicated that the biosensor held good stability. Subsequently, to estimate the selectivity of the biosensor, CTP (100 μM), GTP (100 μM), and TTP (100 μM) were chosen as interfering substances. As shown in Fig. 5B, a relatively low ECL intensity of the CTP, GTP, and TTP was observed, while the ECL intensity of ATP (20 μM) improved observably. What's more, the ECL signal of the mixture comprising the above interferents and ATP was almost consistent with that of the ATP. These results indicated that the biosensor possessed excellent performance for ATP detection.

Application of the biosensor

To assess the application of the biosensor for ATP detection in real samples, recovery tests were performed. A series of ATP concentration was added to 10-fold diluted human serums, and then, the added ATP was tested. The serums were obtained from healthy people. From Table 1, the biosensor showed good recoveries ranging from 91.5 to 106.0 % with acceptable RSD from 1.0 to 9.7 %. This result indicated that the biosensor could be applied to analyze ATP in serum samples.

Conclusion

We have successfully constructed a novel switched ECL biosensor for sensitive detection of ATP assay using the 3D micromolecule walking nanomachine as excellent signal amplification and TiO_2/Ag-ABEI nanoparticles as prominent luminophores. The designed micromolecule walking nanomachine instead of a conventional DNA walker enabled the ATP walker to motion along the preset track, achieving the efficient conversion of an ATP molecule to plentiful output DNA. Moreover, the dual-catalytic effect of TiO_2/Ag NPs toward H_2O_2 is prominently improving the ECL intensity of ABEI. Unlike most of the reported ECL biosensors based on the ABEI/H_2O_2 system, the developed "off-on" ECL biosensor possessed an obvious signal-to-noise ratio as well as higher sensitivity and specificity. And, the biosensor was demonstrated to be successfully applied in detecting ATP in human serums. Significantly, this study offered a novel concept for further expansion of walking nanomachine from DNA walkers to small molecules or proteins walkers.

Table 1 The detection results of target ATP in human serum samples

Sample	Spiked (nM)	Detected (nM)	Recovery (%)	RSD (%)
1	1.0	0.98	98.0	1.0
2	100.0	99.9	99.9	1.1
3	1000.0	915.0	91.5	9.7
4	10000.0	10564.0	106.0	5.8

Supplementary Information The online version contains supplementary material available at https://doi.org/10.1007/s00604-021-04895-x.

Funding This work was funded by financial support from the National Natural Science Foundation of China (82002257, 81702083), the Natural Science Foundation Project of Chongqing (cstc2020jcyj-msxmX0190), the Science and Technology Plan Project of Yuzhong District of Chongqing (20170128), and Hospital-special Fund of Chengdu University of TCM (YYZX20180030).

Declarations

Conflict of interest The authors declare that they have no competing interests.

References

1. Chen JY, Liu YC, Ji XH, He ZK (2016) Target-protecting dumbbell molecular probe against exonucleases digestion for sensitive detection of ATP and streptavidin. Biosens Bioelectron 83:221–228

2. Gourine AV, Llaudet E, Dale N, Spyer KM (2005) ATP is a mediator of chemosensory transduction in the central nervous system. Nature 436:108–111
3. Fan YY, Mou ZL, Wang M, Li J, Zhang J, Dang FQ, Zhang ZQ (2018) Chimeric aptamers-based and MoS_2 nanosheet-enhanced label-free fluorescence polarization strategy for adenosine triphosphate detection. Anal Chem 90:13708–13713
4. Gorman MW, Feigl EO, Buffington CW (2007) Human plasma ATP concentration. Clin Chem 53:318–325
5. Zhang XY, Song CX, Yang K, Hong WW, Lu Y, Yu P, Mao LQ (2018) Photo-induced regeneration of an aptamer-based electrochemical sensor for sensitively detecting adenosine triphosphate. Anal Chem 90:4968–4971
6. Lu SS, Wang S, Chen CX, Sun J, Yang XR (2018) Enzyme-free aptamer/AuNPs-based fluorometric and colorimetric dual-mode detection for ATP. Sens Actuators B-Chem 265:67–74
7. Huang YF, Chang HT (2007) Analysis of adenosine triphosphate and glutathione through gold nanoparticles assisted laser desorption/ionization mass spectrometry. Anal Chem 79:4852–4859
8. Xue XF, Wang F, Zhou JH, Chen F, Li Y, Zhao J (2009) Online cleanup of accelerated solvent extractions for determination of adenosine 5'-triphosphate (ATP), adenosine 5'-diphosphate (ADP), and adenosine 5'-monophosphate (AMP) in royal jelly using high-performance liquid chromatography. J Agric Food Chem 57:4500–4505
9. Huang LX, Guo Q, Chen Y, Verwilst P, Son SB, Wu JB, Cao QY, Kim JS (2019) Nanomolar detection of adenosine triphosphate (ATP) using a nanostructured fluorescent chemosensing ensemble. Chem Commun 55:14135–14138
10. Li X, Yang JM, Xie JQ, Jiang BY, Yuan R, Xiang Y (2018) Cascaded signal amplification via target-triggered formation of aptazyme for sensitive electrochemical detection of ATP. Biosens Bioelectron 102:296–300
11. Liu YT, Lei JP, Huang Y, Ju HX (2014) "off-on" electrochemiluminescence system for sensitive detection of ATP via target-induced structure switching. Anal Chem 86:8735–8741
12. Ma W, Xu LG, de Moura AF, Wu XL, Kuang H, Xu CL, Kotov NA (2017) Chiral inorganic nanostructures. Chem Rev 117:8041–8093
13. Karimi A, Husain SW, Hosseini M, Azar PA, Ganjali MR (2020) A sensitive signal-on electrochemiluminescence sensor based on a nanocomposite of polypyrrole-Gd_2O_3 for the determination of L-cysteine in biological fluids. Microchim Acta 187:398–407
14. Lu LX, Yuan W, Xiong Q, Wang MH, Liu YJ, Cao M, Xiong XH (2021) One-step grain pretreatment for ochratoxin A detection based on bipolar electrode- electrochemiluminescence biosensor. Anal Chim Acta 1141:83–90
15. Azam NFN, Mohd-Naim NF, Kurup CP, Ahmed MU (2020) Electrochemiluminescence immunosensor for tropomyosin using carbon nanohorns/Nafion/Fe_3O_4@Pd screen-printed electrodes. Microchim Acta 187:456–465
16. Lu LP, Liu C, Miao WJ, Wang XY, Guo GS (2020) Ultrasensitive detection of miRNA based on efficient immobilization of probe and electrochemiluminescent quenching of $Ru(bpy)_3^{2+}$ by methylene blue. Anal Chim Acta 1093:52–60
17. Ma C, Cao Y, Gou XD, Zhu JJ (2020) Recent progress in electrochemiluminescence sensing and imaging. Anal Chem 92:431–454
18. Li SK, Liu ZT, Li JY, Chen AY, Chai YQ, Yuan R, Zhuo Y (2018) Enzyme-free target recycling and double-output amplification system for electrochemiluminescent assay of mucin1 with MoS_2 nanoflowers as co-reaction accelerator. ACS Appl Mater Interfaces 10:14483–14490
19. Yang F, Jiang XY, Zhong X, Wei SP, Yuan R (2018) Highly sensitive electrochemiluminescence detection of mucin1 based on V_2O_5 nanospheres as peroxidase mimetics to catalyze H_2O_2 for signal amplification. Sens Actuators B-Chem 265:126–133
20. Xu LH, Li JJ, Zeng HB, Zhang XJ, Cosnier S, Marks RS, Shan D (2019) ATMP-induced three-dimensional conductive polymer hydrogel scaffold for a novel enhanced solid-state electrochemiluminescence biosensor. Biosens Bioelectron 143:111601–111608
21. Li J, Jiang D, Shan X, Wang W, Chen Z (2020) An "off-on" electrochemiluminescence aptasensor for microcystin-LR assay based on the resonance energy transfer from PTCA/NH_2-MIL-125(Ti) to gold nanoparticles. Microchim Acta 187:474–483
22. Wang HQ, Ma ZF (2019) "off-on" signal amplification strategy amperometric immunosensor for ultrasensitive detection of tumour marker. Biosens Bioelectron 132:265–270
23. Gao XS, Li HK, Zhao Y, Jie GF (2019) Triple-helix molecular switch-based versatile "off-on" electrochemiluminescence and fluorescence biosensing platform for ultrasensitive detection of lipopolysaccharide by multiple-amplification strategy. Biosens Bioelectron 143:111602–111610
24. Qu XM, Zhu D, Yao GB, Su S, Chao J, Liu HJ, Zuo XL, Wang LH, Shi JY, Wang LH, Huang W, Pei H, Fan CH (2017) An exonuclease III-powered, on-particle stochastic DNA walker. Angew Chem Int Ed 56:1855–1858
25. Lu HW, Tang HL, Yi XY, Wang JX (2020) Three-dimensional DNA nanomachine combined with toehold-mediated strand displacement reaction for sensitive electrochemical detection of MiRNA. Langmuir 36:10708–10714
26. Qi XJ, Lu CH, Liu XQ, Shimron S, Yang HH, Willner I (2013) Autonomous control of interfacial electron transfer and the activation of DNA machines by an oscillatory pH system. Nano Lett 13:4920–4924
27. Thubagere AJ, Li W, Johnson RF, Chen ZB, Doroudi S, Lee YL, Izatt G, Wittman S, Srinivas N, Woods D, Winfree E, Qian LL (2017) A cargo-sorting DNA robot. Science 357:6356–6358
28. Li DD, Xu YX, Fan L, Shen B, Ding XJ, Yuan R, Li XM, Chen WX (2020) Target-driven rolling walker based electrochemical biosensor for ultrasensitive detection of circulating tumor DNA using doxorubicin@tetrahedron-Au tags. Biosens Bioelectron 148:111826–111833
29. Xiao MS, Zou K, Li L, Wang LH, Tian Y, Fan CH, Pei H (2019) Stochastic DNA walkers in droplets for super-multiplexed bacterial phenotype detection. Angew Chem Int Ed 58:15448–15454
30. Xu MD, Zhuang JY, Jiang XY, Liu XZ, Tang DP (2019) A three-dimensional DNA walker amplified FRET sensor for detection of telomerase activity based on the MnO_2 nanosheet-upconversion nanoparticle sensing platform. Chem Commun 55:9857–9860
31. Fakhari F, Rokita SE (2014) A walk along DNA using bipedal migration of a dynamic and covalent crosslinker. Nat Commun 5:5591–5601
32. Jung C, Allen PB, Ellington AD (2017) A simple, cleated DNA walker that hangs on to surfaces. ACS Nano 11:8047–8054
33. Wang L, Liu PF, Liu ZJ, Zhao KR, Ye SY, Liang GX, Zhu JJ (2020) Simple tripedal DNA walker prepared by target-triggered catalytic hairpin assembly for ultrasensitive electrochemiluminescence detection of microRNA. ACS Sens 5:3584–3590

34. Yang XL, Tang YN, Mason SD, Chen JB, Li F (2016) Enzyme-powered three-dimensional DNA nanomachine for DNA walking, payload release, and biosensing. ACS Nano 10:2324–2330
35. Wang CQ, Liu R, Hu JY, Lv Y (2019) Ratiometric DNA walking machine for accurate and amplified bioassay. Chem- Eur J 25: 12270–12274
36. Murphy CJ, Chang HH, Falagan-Lotsch P, Gole MT, Hofmann DM, Hoang KNL, McClain SM, Meyer SM, Turner JG, Unnikrishnan M, Wu M, Zhang X, Zhang YZ (2019) Virus-sized gold nanorods: plasmonic particles for biology. Acc Chem Res 52: 2124–2135
37. Li Q, Liang XH, Mu XM, Tan L, Lu JN, Hu K, Zhao SL, Tian JN (2020) Ratiometric fluorescent 3D DNA walker and catalyzed hairpin assembly for determination of microRNA. Microchim Acta 187:365–374